frontiers in Earth Science

ORIGINAL RESEARCH
published: 12 December 2018
doi: 10.3389/feart.2018.00232

Impact of Wave Number Choice in Spectral Nudging Applications During a South Atlantic Convergence Zone Event

Natália Pillar da Silva and Ricardo de Camargo**

Instituto de Astronomia, Geofísica e Ciências Atmosféricas, Universidade de São Paulo, São Paulo, Brazil

Several studies showed the advantages of using nudging techniques to enforce the evolution of a numerical model to approximate large-scale features to a reference. Spectral nudging applications are particularly useful since they also provide the ability to maintain higher temporal and spatial variability in the simulations results. In this study, different nudging configurations are tested for an intense South Atlantic Convergence Zone (SACZ) event. Large-scale features directly modulate the SACZ formation and persistence. Therefore, the employment of relaxation methods enhances the representation of continental-wide features from lateral boundary conditions over the interior of broad domains. Results show that Spectral Nudging is very effective at imposing the selected synoptic scales onto the solution, while allowing the limited-area model to incorporate finer-scale features. Wave numbers with associated length scales of 2000km are ideal to enforce large-scale fields to represent features important for the SACZ formation and persistence. Using larger wave numbers can improve the simulation performance, but at a cost of damping the model dynamic and physical contribution to the final solution.

Keywords: numerical modeling, spectral nudging, South Atlantic Convergence Zone, regional climate, model evaluation

OPEN ACCESS

Edited by:
Raquel Nieto,
University of Vigo, Spain

Reviewed by:
Chenghai Wang,
Lanzhou University, China
Benjamin Schaaf,
Helmholtz Centre for Materials and Coastal Research (HZG), Germany

****Correspondence:***
Natália Pillar da Silva
natalia.pillar@gmail.com
Ricardo de Camargo
ricamarg@model.iag.usp.br

Specialty section:
This article was submitted to Atmospheric Science, a section of the journal Frontiers in Earth Science

Received: *09 April 2018*
Accepted: *29 November 2018*
Published: *12 December 2018*

Citation:
Silva NP and Camargo R (2018) Impact of Wave Number Choice in Spectral Nudging Applications During a South Atlantic Convergence Zone Event. Front. Earth Sci. 6:232. doi: 10.3389/feart.2018.00232

1. INTRODUCTION

The South Atlantic Convergence Zone (SACZ) is one of the main components of the South American Monsoon System (SAMS, Zhou and Lau, 1998) and it is characterized as a persistent cloudiness band with northwest-southeast orientation, predominant during summertime in South America (Kodama, 1992, 1993), that significantly affects the precipitation regime over southeastern Brazil. The system SAMS/SACZ exhibits a broad temporal variability over several scales and its positioning and intensity are modulated by large-scale atmospheric features, as described in several extensive reviews (Gan et al., 2005; Vera et al., 2006; Marengo et al., 2012). In this context, the SACZ predictability becomes particularly challenging in regional numerical studies for events ranging from a sub-seasonal scale to climate studies (Bombardi and Carvalho, 2011).

One way to improve the regional representation of local features is to use a dynamical downscaling approach (Dickinson et al., 1989), where large-scale atmospheric fields from a coarser dataset are input for regional climate models. This process yields solutions driven by the large-scale data and with features generated by the internal physics and dynamics of the regional modeling

system. For longer numerical experiments the inflow of information in the model boundaries can produce errors and increase results uncertainty. And, according to Davies and Turner (1977) and Davies (1983), in regional grids with larger domains, the solution provided by the model can diverge significantly from global analysis datasets. To mitigate this effect, a nudging process is applied in many regional climate applications. This method basically relaxes the solution provided by the model to a reference value at any grid point (Stauffer and Seaman, 1990). The solution is, therefore, constrained by this reference field. Recently, the use of spectral nudging, a variation of the classical nudging approach, has been used (Miguez-Macho et al., 2004; Vincent and Hahmann, 2015; Gómez and Miguez-Macho, 2017) so only a part of the total spectrum is relaxed toward the solution given by the reference fields. Therefore, the user can apply the nudging for large-scale features and allow the model to generate the solution for smaller scales.

Spectral nudging investigations were first performed by Waldron et al. (1996), that introduced the use of spectral nudging in Limited Area Models (LAMs) to incorporate large scale features in the inner LAM and eliminate computational modes in a domain with complex topography over the Great Basin of the western United States for an intense winter case study. The authors applied a Fourier filter to prevent computational modes given by the use of an unstaggered grid along with spectral nudging in the interior grid of the Utah LAM model for wavenumbers ranging from 0 to 6. von Storch et al. (2000), using the regional climate model REMO, provided a January-March 1993 application of spectral nudging for zonal and meridional wind components over the Western Europe region and demonstrated that, when input from the reference fields are incorporated only by the lateral boundary, internal modes can interact with the represented large-scale fields and significantly increase bias. The authors implement a height-dependent nudging factor to evaluate different wave numbers in different pressure levels. Since numerical experiments in subseasonal, seasonal and regional climate scales show sensibility to domain positioning and size, to reduce dependency on those factors, Miguez-Macho et al. (2004) suggested the use of spectral nudging for large-scale atmospheric features (larger than 2500 km) and constrain the synoptic scales in the Regional Amospheric Modeling System (RAMS) model solution to the reanalysis data while still allowing the model dynamics to contribute in smaller scales representation during a June 2000 case over a North America domain. In a later research, Miguez-Macho et al. (2005) investigated how a spectral nudging application of large-scale features (also for wavelengths larger than 2500 km), along with improved soil data, enhanced the precipitation representation by the RAMS model for a regional climate simulation over North America. Wang and Kotamarthi (2013) tested different spectral nudging approaches in the Nested Regional Climate Model (NRCM) and stated that using the nudging six waves for the whole simulation period above the 850hPa level improved the performance of the regional climate model in more than 30% when compared to a test case with no nudging being used. Using techniques similar to those presented by Miguez-Macho et al. (2004, 2005), the authors applied spectral nudging to temperature, horizontal winds and geopotential above the Planetary Boundary Layer (PBL) to avoid damping near surface interactions by the model. Vincent and Hahmann (2015) evaluated the nudging effect on wind speed variance through grid and spectral nudging tests using the WRF model for three case studies over the Baltic Sea region during the year 2000. A short 36h simulation without nudging applied was performed for a control case, along with two longer simulations with a grid and spectral nudging application for a test of the procedure influence. In both test cases, nudging was applied to the U and V wind components, potential temperature, and geopotential. The spectral test was used only for wavelengths longer than 250km in both zonal and meridional directions. The authors' argue that even though nudging applications can improve the mean flow representation, it can also impact the model resolved variance, which can be crucial in wind energy studies that use wind speed distributions for energy production calculations. Besides, Gómez and Miguez-Macho (2017) tested the WRF model sensibility to different cut-off wave numbers and spin-up times for short experiments over North America and verified that the approach is effective in enforcing the synoptic scales into the numeric solution while allowing the model to contribute in smaller scales. The authors show that the model errors rapidly decrease when cut-off wave numbers equivalent to length-scales of around 1000 km are used. This scale coincide with the Rossby radius of deformation, which indicates the separation between synoptic and convective scales in the atmospheric flow (Gómez and Miguez-Macho, 2017).

This application can be particularly useful for the representation of SACZ events since the large-scale mean flow plays an important role in the persistence of the convergence zone. Also, for larger domains applications, the mean flow provided by the LBC may not be sufficient for a proper representation of continental wide features that impact the SACZ formation and persistence. Therefore, nudging applications can ensure the proper conditions for such events in a sub-seasonal scale. In this paper, we describe the application of numerical experiments with the Weather Research and Forecasting System (WRF) model for a particularly intense SACZ event occurred in December 2013. This particular case was selected after we analyzed the *Large-Scale Index for the South American Monsoon* (LISAM - da Silva and de Carvalho, 2007; Carvalho et al., 2011). The spatial pattern of precipitation provided by the second mode of the EOF analysis made for the LISAM calculation indicates the presence of a SACZ with projection toward the South Atlantic ocean. We analyzed the time series of this mode of variability selected cases of SACZ occurrence with high intensity (standard deviation values exceeding 2) and persistence (duration of at least 3 pentads). The 2013 case, from 11 December to 26 December was also responsible for several damages to local communities in the affected areas of the State of Espirito Santo (around 20°*S*). The Brazilian National Center for Natural Disasters Monitoring and Alerts (CEMADEN, https://www.cemaden.gov.br/) registered 52 affected cities, substantial financial losses and 26 deaths caused by floods and mudslides.

We performed tests without any nudging application, using a range of spectral nudging with progressive increase of

wave numbers and a test with grid nudging, representing an application for the whole spectrum. Since the SACZ is an event that is tightly modulated by large scale structures, the spectral nudging application can be useful to ensure important large scale features representation in the domain interior.

2. DATA AND METHODOLOGY

2.1. Data

The Climate Forecast System Reanalysis (CFSR) dataset was used as initial and lateral boundary condition (LBC) for numerical experiments. The CFSR (Saha et al., 2010) is a global reanalysis product from a third generation effort with high resolution and coupled ocean-atmosphere assimilation system, with a 0.5° × 0.5° regular grid, 40 vertical levels and temporal coverage from 1979 to the present.

To assess the overall simulations performance, results were also compared with the European Center for Medium-Range Weather Forecasts (ECMWF) reanalysis dataset ERA-Interim (Dee et al., 2011), a global atmospheric from 1979 to the present, steadily updated, with a state-of-the-art assimilation. The spatial resolution is nearly 80 km (T255 spectral) and has 60 vertical levels from the surface up to 0.1 hPa.

de Quadro et al. (2012) performed comparisons between six reanalysis products (MERRA, ERA- Interim, ERA-40, NCEP 1, NCEP 2 e NCEP CFSR) and five precipitation datasets (SALDAS, CPC, CMAP, GPCP e GLDAS) to assess their performance in the representation of humidity transport and associated precipitation for SACZ documented events ranging from 1979 to 2010. The results suggest that the CFSR reanalysis showed improved results in comparison with the other datasets. Therefore, CFSR data was used to initialize the experiments and for the nudging applications while the ERA-Interim reanalysis was used as a reference for the results evaluation.

Also, to evaluate how the experiments represented the precipitation distribution along the SACZ, the Tropical Rainfall Measuring Mission (TRMM) data was used (Huffman et al., 2007). This mission was designed provide monitoring alternatives for subtropical and tropical precipitation. Here, we used the TRMM Multi-satellite Precipitation Analysis (TMPA) 3B42 daily product with 0.25 deg horizontal resolution.

2.2. Model Configuration

The WRF v.3.9 model is a fully compressible, nonhydrostatic modeling system with an Eulerian dynamical core (Skamarock and Klemp, 2008). There are two dynamical cores available, and in the present work, we used the Advanced Research WRF (ARW) core, developed and continuously supported by the National Center for Atmospheric Research (NCAR). The WRF-ARW core includes multiple parameterization options for multiple physics suites. Time integration is performed with a 3rd-order Runge-Kutta scheme. The model was designed to provide conservation of mass and momentum and uses flux form prognostic equations. The vertical coordinates consists of a terrain following hydrostatic pressure system. The time period simulated ranged from from 0000UTC 26 November 2013 to 0000UTC 10 January 2014, contemplating 15 days prior and posterior to the SACZ cased under investigation. This period was selected in order to provide a numerical study of this persistent case in a subsesasonal scale, so that the relaxation influence throughout a longer simulated period could be verified. All simulations were integrated in a Mercator grid, illustrated in **Figure 1** with 25 km horizontal resolution, a center positioned in 10° W latitude and 56° W longitude, 320 points in the east-west direction (8000 km), 300 points in the north-south direction (7500 km), 40 vertical levels and 50 hPa at the top of the numerical grid. To ensure stability, a timestep of 60 s was used and outputs were obtained every 6 h. The physical parameterization options for all experiments and their main references are summarized in **Table 1**.

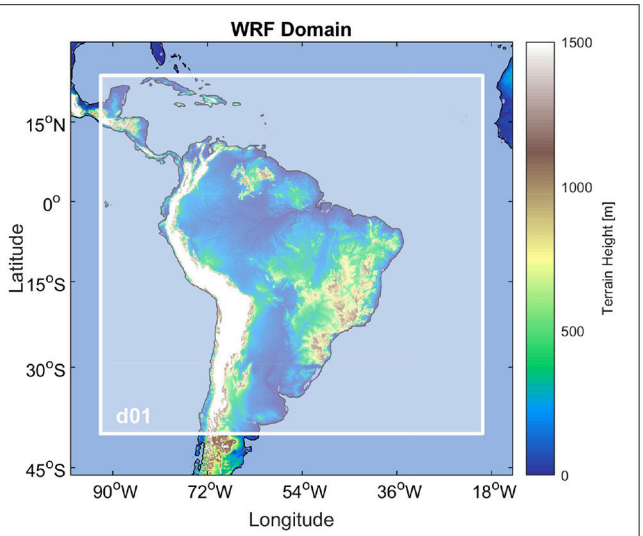

FIGURE 1 | WRF Domain for all numerical experiments are represented in the white shaded area and labeled by d01. The map illustrates the terrain height (in meters) for continental areas. The Andes mountain height is saturated in the map in order to highlight the central Brazil topography.

TABLE 1 | Physical parameterization options used in all experiments and their main references.

Physical parameterization	Option	Reference
Microphysics	WRF single-moment 6-class	Hong and Lim, 2006
Cumulus	Kain-fritsch	Kain, 2004
Longwage radiation	CAM3	Collins et al., 2004
Shortwave radiation	CAM3	Collins et al., 2004
Surface layer	MM5	Zhang and Anthes, 1982
Planetary boundary layer	Yonsei University	Hong and Lim, 2006
Land surface	Noah-MP	Niu et al., 2011

2.3. Nudging Technique

The nudging process, also known as Newtonian relaxation, relaxes the model solution toward a reference. In the WRF model, the procedure follows Stauffer and Seaman (1990) and it is

described in the technical documentation Skamarock and Klemp (2008).

The spectral nudging process applied in the present study follows equation 1, in which a spectral filter (in both x and y directions) is applied to $(\hat{\theta_0} - \theta)$ without filtering in the vertical direction. For the grid nudging technique, a similar approach to equation 1 is used, without the filtering term.

$$\frac{\partial \theta}{\partial t} = F(\theta) + G_\theta W_\theta F_{xy}(\hat{\theta_0} - \theta) \quad (1)$$

The θ value represents the variable being relaxed toward the reference datasset. The spectral filter F_{xy} cancel frequencies that lie above the cut-off wave number, and this ensures that only certain wavelengths are used in the nudging procedure. Gómez and Miguez-Macho (2017) point out that when the cut-off wave number considers the uppermost possible frequency, the F_{xy} parameter in Equation 1 provides a complete FFT then an inverse FFT and the spectral nudging procedures becomes equivalent to the grid nudging application. The authors present results that indicate a grid nudging application as an asymptotic case of the spectral nudging. The choice of a proper cut-off wave number was topic of discussion in several studies. Miguez-Macho et al. (2004) used the lowest possible wave number to ensure only the largest scales were being relaxed and, therefore, guaranteeing minimum interference of the nudging procedure in the model solution. This relationship was summarized by the authors in the Equation 2:

$$n = \frac{D_{x,y} N_{x,y}}{R} + 1 \quad (2)$$

In Equation 2, n is the wave number for x, y directions, $D_{x,y}$ represents the model resolution, $N_{x,y}$ is equal to the number of grid points in both directions, and finally R represents the Rossby radius value. In their examples, the $1000km$ value showed better results.

2.4. Experiments Configuration

Seven numerical experiments with the WRF model were performed with different nudging options. We evaluated how numerical results depend on the nudging type and strength following framework presented in **Table 2**. As stated in Gómez and Miguez-Macho (2017), a free run (*ndgnone*) and a grid nudging utilization (*ndggrid*) represent asymptotic solutions for the spectral nudging procedure described by Equation 1. Besides these tests, we examined spectral nudging experiments with cut-off wave numbers related to fundamental length scales in the present study structure: 8000 km (*ndg8000*)—approximate domain dimension as the less restrictive spectral nudging case; 1000 km (*ndg1000*)—the Rossby radius length for most mesoscale studies; 500 km (*ndg0500*)—a fair representation of the reference dataset (CFSv2) effective resolution. The other tests cover intermediate lengths between those values (*ndg4000*, *ndg2000*). All simulations were configured with a nudging coefficients of $3.0 \times 10\_4 s^{-1}$ (approximately 1 h). Relaxation was activated in all experiments, except for *ndgnone*. Gómez and Miguez-Macho (2017) discuss that is not recommended to nudge variables in the Planetary Boundary Layer (PBL), since surface characteristics in the model differ from global reanalysis datasets used as LBC. Therefore, we only nudge variables above the PBL layer and, since the SACZ is mainly driven by humidity convergence in low levels, we chose to not apply nudging in humidity allowing more freedom for the numerical model contribution. Nudging was applied in zonal and meridional wind components, geopotential height and temperature fields, above the PBL (automatically defined by the numerical model at each time step) throughout the complete integration period every 6 h. The experiments aim to provide input on the WRF model sensibility to the wave number selection when using spectral nudging for a SACZ case.

TABLE 2 | Wave numbers used in spectral nudging options for all experiments in both x and y direction and the associated lengths, in km.

Experiment	WN_x	WN_y	Description
ndgnone	–	–	Free run
ndg8000	2	2	Approximate domain size
ndg4000	3	3	Intermediate length scale
ndg2000	5	5	Intermediate length scale
ndg1000	9	9	Approximate Rossby radius length
ndg0500	17	16	Effective resolution of reference data
ndggrid	–	–	Grid nudging

2.5. Evaluation

The results evaluation were based on the comparison between numerical estimates and reanalysis products. Contrasting model output with the CFSR data provide information about how each experiment deviates from the reference value in the nudging applications. This comparison is particularly useful to assess if the model dynamical and physical cores still contribute to the numerical solution while the large scale features are enforced by the reference. While contrasting the experiments results with the ERA-Interim dataset, we can determine the overall performance of the tests. This is done by calculating the Root Mean Square Deviation, that represent the standard deviation of residuals, i.e. prediction errors.

$$RMSD = \sqrt{\sum_{i=1}^{N} \frac{(z_{f_i} - z_{o_i})^2}{N}} \quad (3)$$

In the equation 3, z_f corresponds to valuables predicted by the model, z_o are observations, while i is the position of the values in the grid with N values. This calculation was made for both space, in a comparison between each grid point at all time steps, and time, in a comparison of errors in all time steps for each grid point. We also evaluate the experiments performance by comparing the spatial spectra of kinetic energy for all experiments. The kinetic energy provides a way to evaluate both zonal and meridional wind components with one scalar value. Wind component fields were detrended and pre-processed to ensure periodicity according to Errico (1985). And power spectrum as calculated using the guidelines offered by Vincent and Hahmann (2015).

$$S(k) = \frac{2}{C_w N f_s} |A(k)|^2 \quad (4)$$

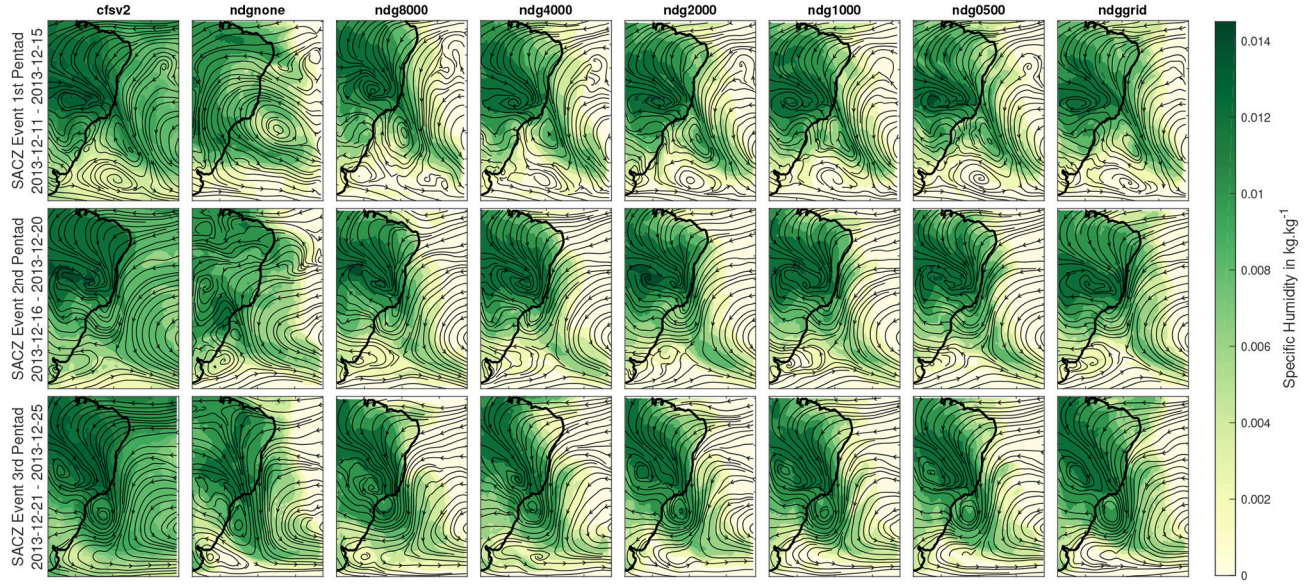

FIGURE 2 | Specific humidity (filled contours, in kg/kg) and streamlines at 850 hPa. Top, middle and bottom rows show averages calculated for the first, second and third pentads of the SACZ event, respectively.

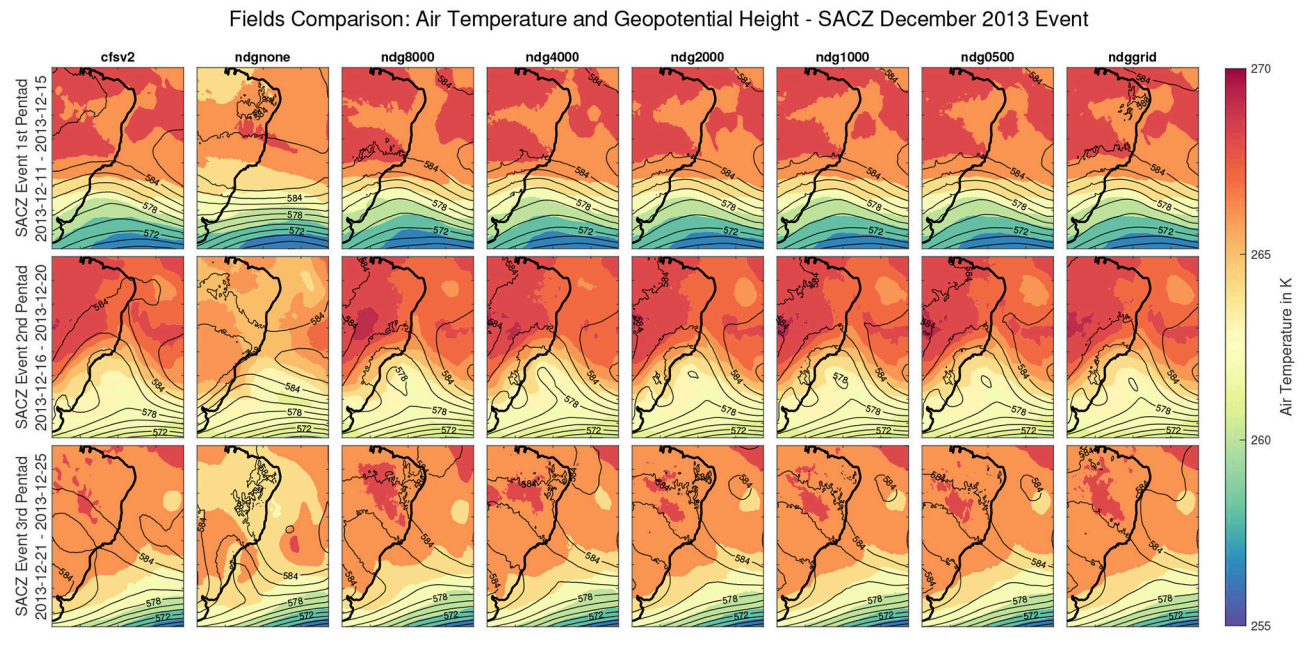

FIGURE 3 | Temperature (filled contours, in K) and geopotential height (black contours, in m) at 500 hPa. Top, middle, and bottom rows show averages calculated for the first, second and third pentads of the SACZ event, respectively.

Where $A(k)$ represents the Fourier coefficients of the variable in study, N is the length of the series, k ranges from $0 \leqslant k \leqslant N/2$, and f_s is the sampling resolution, i.e. $1/dx$, where dx is the horizontal grid spacing. And the C_w corresponds to a correction for the window function, given by Vincent and Hahmann (2015):

$$C_w = \frac{1}{N}\sum_{j=0}^{N-1} W^2(j) \tag{5}$$

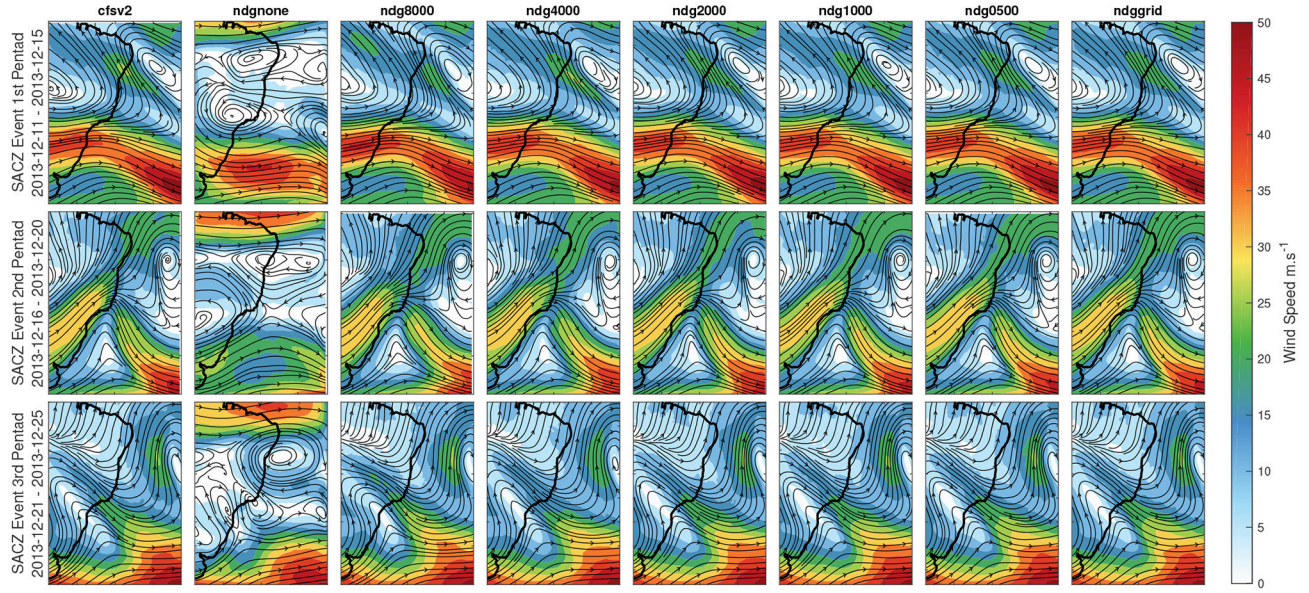

FIGURE 4 | Wind speed (filled contours, in $m.s^{-1}$) and streamlines at 200 hPa. Top, middle and bottom rows show averages calculated for the first, second and third pentads of the SACZ event, respectively.

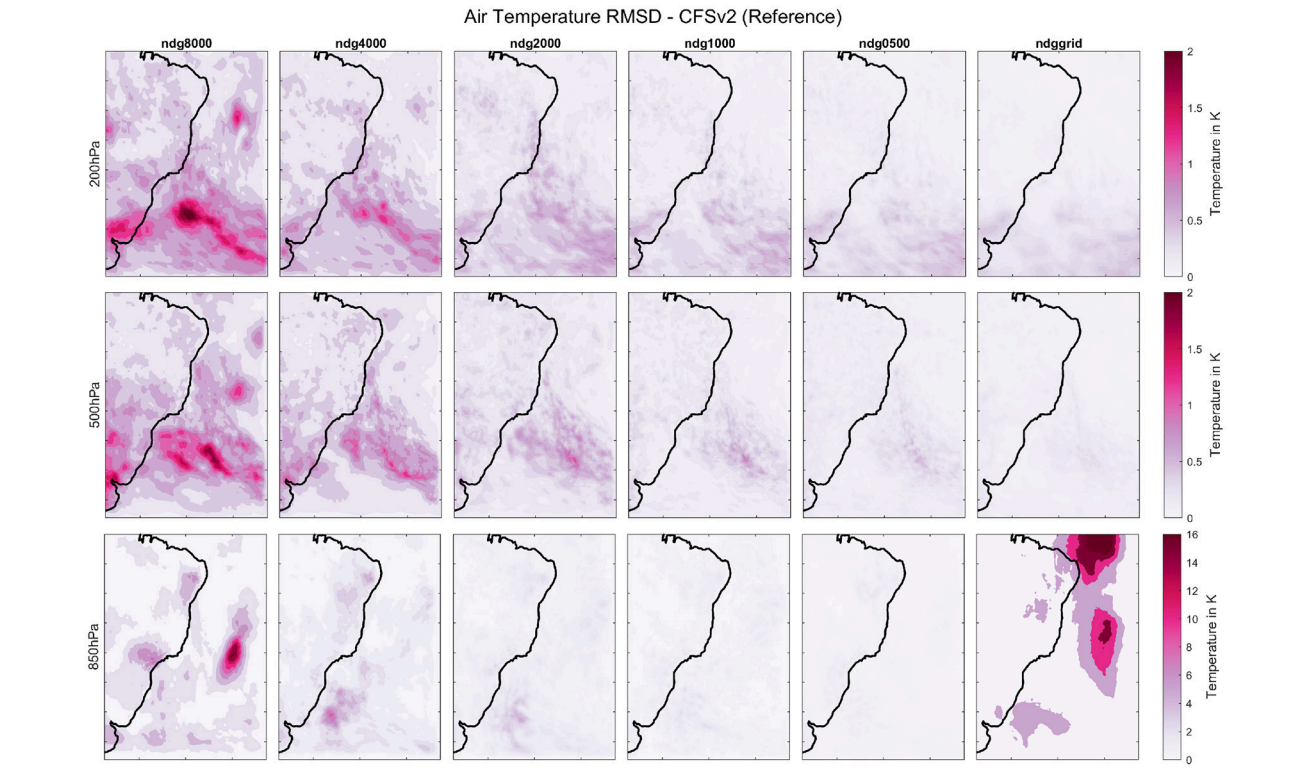

FIGURE 5 | RMSD of temperature values during the SACZ event. Maps of all numerical experiments (columns) for upper levels (200 hPa, top row), middle levels (500 hPa, middle row) and lower levels (850 hPa, bottom row) are shown.

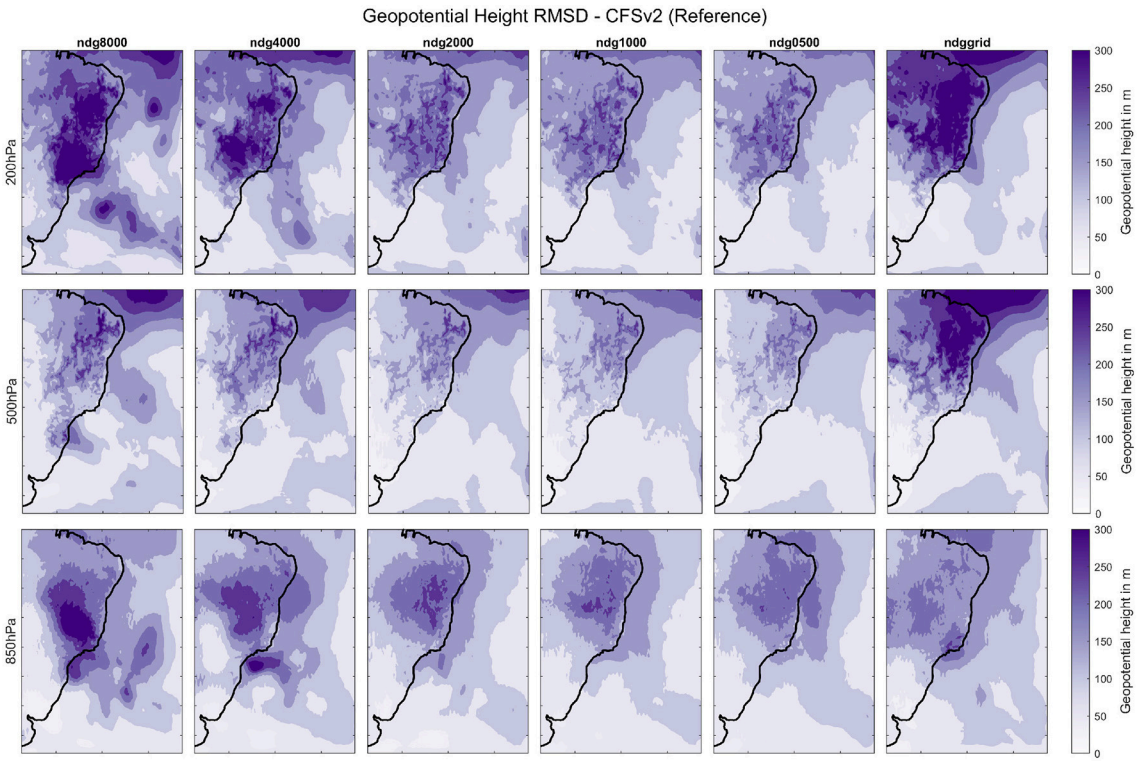

FIGURE 6 | RMSD of geopotential height values during the SACZ event. Maps of all numerical experiments (columns) for upper levels (200 hPa, top row), middle levels (500 hPa, middle row) and lower levels (850 hPa, bottom row) are shown.

Calculations are performed for the vertical levels: near surface (2-m or 10-m above ground), 850, 500, and 200 hPa. In the near-surface levels lower levels (850 hPa), there was no direct influence of the nudging procedures while the middle and upper levels have solutions constrained by the CFSR reanalysis data.

3. RESULTS AND DISCUSSION

3.1. Nudging Effect

3.1.1. Pressure Levels

We analyzed the numerical representation of this particular event through the comparison between spatial fields in three levels (lower 850hPa, middle 500hPa, and upper 200hPa) of relaxed variables and specific humidity, given the importance for the SACZ characterization. **Figure 2** shows the specific humidity fields along with streamlines distribution during three pentads of the event in lower levels (850hPa). It can be seen that without the application of nudging in the interior domain, large scale fields are completely distorted for all periods and, given the lack of a large scale structure, the SACZ cannot be properly represented by the model. This distortion results from errors propagating from the lateral boundary conditions toward the domain center. Miguez-Macho et al. (2004) describe similar issues for numerical experiments over North America and argues favorably toward the use of nudging procedures to avoid this obstacle. Indeed, the addition of nudging procedures, in all cases, provide significantly better results and the low level humidity convergence that supports the SACZ is represented. When compared to the CFSv2 data, all of the experiments underestimate the humidity in oceanic regions. This is an expected outcome, since humidity was not nudged into the solutions and, therefore, all of this information is incorporated into the model domain by the LBC data. There are some visible differences between experiments with different nudging configurations for each displayed pentad, mostly related to the positioning of dynamical structures around the convergence zone.

In the middle atmosphere (**Figure 3**), geopotential and temperature fields exhibit larger differences between the reference and the *ndgnone* experiment, which follows results in lower levels and corroborates the use of nudging to ensure large-scale features representation for the SACZ development. In both reference and nudging experiment fields, there is a trough above the lower levels cyclonic vortex structure responsible for the SACZ persistent positioning in early stages of development. During the second pentad, this feature is intensified and nudging numerical results even show a closed cyclonic feature following the lower level structure. This vertical support for the cyclonic feature at lower levels is only present in the spectral/gridded nudging experiments, which is a good indication that the model still contributes to the numerical solution even when both temperature and geopotential height are being nudged.

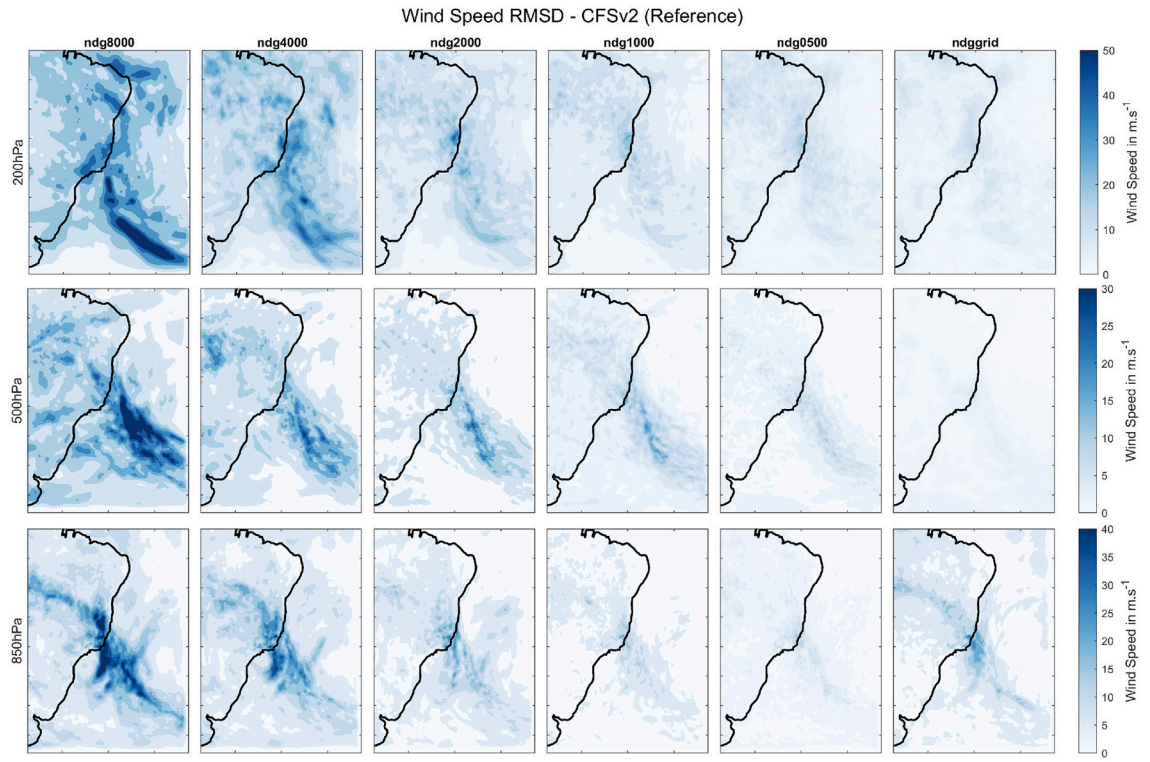

FIGURE 7 | RMSD of wind speed values during the SACZ event. Maps of all numerical experiments (columns) for upper levels (200 hPa, top row), middle levels (500 hPa, middle row) and lower levels (850 hPa, bottom row) are shown.

For upper levels (200 hPa, **Figure 4**), the circulation patterns show a large distortion for the *ndgnone* experiment, and the main features that contribute to the SACZ permanence are not generated by the model. The high pressure center above Bolivia and a trough over northeastern Brazil are well formed for all the nudging experiments and generally follow the reference fields for the whole simulation period. Wind speed and streamlines of the reference maps show upper-level structures for the convergence zone formation particularly from the second pentad (middle panels in **Figure 4**) onwards. The trough formation over the lower levels cyclonic vortices also offer support for the SACZ development and formation. As found in other levels, the *ndgnone* experiment failed to provide dynamical guidance for the convergence zone formation due to errors propagating from lateral boundaries and amplifying toward the domain interior. All nudging experiments exhibit higher resemblance with the reference field in this level, which is expected given the relaxation procedure configuration.

3.1.2. Spatial Spectra of Kinetic Energy

To further explore how nudging experiments deviate from reference fields, we calculated the RMSD maps throughout the domain during the SACZ event for relaxed variables in all experiments using nudging. **Figure 5** illustrates the results for air temperature at upper (200 hPa, top row), middle (500 hPa, central row) and lower (850 hPa, bottom row) levels. It is clear that a decrease in the scale length used for the relaxation method yields in RMSD reduction toward almost null values for most *ndggrid* cases. More restrictive nudging applications damp the model contribution for the final solution and the simulation becomes basically a more refined version of the reference field. Although this can be found for upper and middle levels, the same does not apply in lower levels in the *ndgnone* case, given the considerable RMSD values found in the northern part of the domain. A similar analysis was done for geopotential height values (**Figure 6**). Unlike results for temperature values, in this case, high RMSD values persist in significant levels even for experiments with intense nudging and, as found for temperature maps, the *ndggrid* experiment showed larger RMSD values in comparison to other configurations. We also conducted this analysis for wind speed fields (**Figure 7**). Unlike results for the other nudged variables, wind fields show an expected result for this application: RMSD values reaching almost null amounts with increasing intensity in nudging configurations. Most of the errors persist over the SACZ activity area and the least strong nudging application to generate important results is the *ndg2000*.

The energy transition between larger and mesoscales was analyzed by computing the spatial kinetic energy spectra for all numerical experiments during the SACZ event, along with the reference dataset used for the nudging applications (CFSv2) and an independent reanalysis (ERA-Interim) for general evaluation of performance. **Figure 8** illustrates the

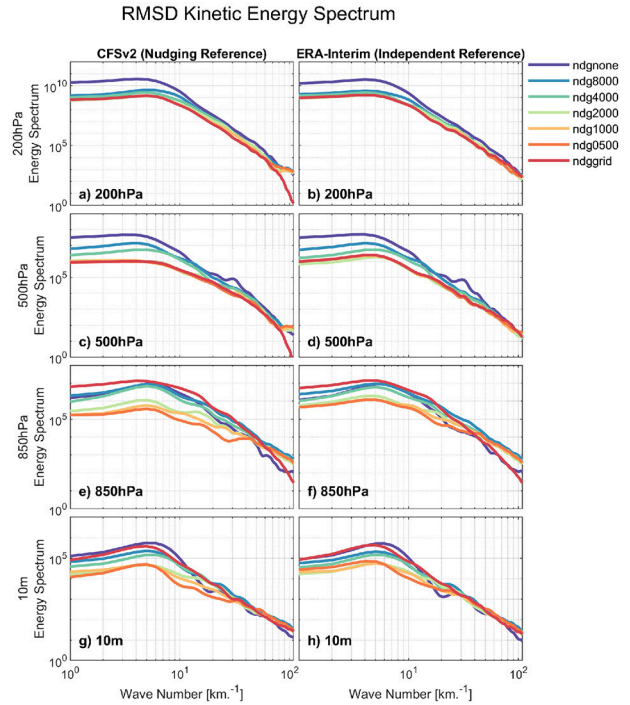

FIGURE 8 | Root Mean Square Deviation (RMSD) of the kinetic energy (in m^2/s^2) calculated using the CFSv2 reanalysis (left) and the ERA-Interim reanalysis (right) for the SACZ case study. **(a,b)** Show top-level (200 hPa) results, **(c,d)** Show middle-level (500 hPa) results, **(e,f)** Show lower-level (850 hPa) results, **(g,h)** Show near-surface (10 m) results.

RMSD of the spatial spectra of kinetic energy from near-surface levels (10m), lower atmosphere (850 hPa), middle atmosphere (500hPa) and upper levels (200 hPa). In general, the application of nudging improved results in all experiments, except for the grid nudging test (*ndggrid* - red line) that showed RMSD values exceeding the free run application if lower levels (**Figures 8f,h**). This is also an indication that the wave number selection in spectral nudging applications can affect the energy dissipation pattern from larger scales to mesoscales with considerable effects in levels not directly influenced by the relaxation technique. Also, this can indicate that the numerical model contributes differently for the final solution given various nudging frameworks. This pattern is also verified in upper levels, but the range between the RMSD curves are not as apparent.

The features presented support the argument that the nudging application was indispensable for the generation of large-scale features capable of supporting the SACZ for the whole event. Some differences between the nudged fields imply that, to allow the model dynamic and physical modules to contribute to the solution, it is important to not enforce the solution to be approximated to the reference in the whole spectrum. Using an option with intermediate restriction and smaller wave numbers (larger scales, 2000km) is enough to fulfill this balance.

TABLE 3 | RMSE during the SACZ event for near surface variables: precipitation (P), air-temperature at 2 m (T_2), specific humidity at 2 m (q_2) and zonal (u_{10}) and meridional (v_{10}) components of the wind at 10 m.

EXP	P	T_{2m}	q_{2m}	u_{10m}	v_{10m}
ndgnone	12.510	3.625	5.091	2.694	2.838
ndg8000	12.532	2.742	4.676	2.184	2.656
ndg4000	12.106	2.738	4.727	2.038	2.406
ndg2000	11.715	2.659	**4.576**	1.849	2.093
ndg1000	12.150	**2.643**	4.652	1.775	2.025
ndg0500	12.656	2.654	4.984	**1.726**	**1.987**
ndggrid	**11.653**	3.283	4.981	1.898	2.164

Results from experiments using a nudging coefficients of 3 × $10^{-4}s^{-1}$. Bold numbers indicate minimum values of RMSE for each variable in all experiments.

3.1.3. Overall Performance

For the evaluation of the overall performance of the numerical experiments, we also calculated the RMSD of fundamental variables associated with the SACZ in near-surface levels using the ERA-Interim dataset (independent reference): precipitation (P), air temperature at 2 m (T_{2m}), specific humidity at 2 m (q_{2m}), and zonal (u_{10m}) and meridional (v_{10m}) wind components at 10 m. Model results were compared to references given by rainfall estimates from TRMM and other surface variables from the ERA-Interim reanalysis dataset. We focus our analysis on our analysis on near-surface variables since there is no direct influence of the relaxation procedure below the PBL. Therefore, the differences between these sets of experiments may represent the model contribution to the final solution through its dynamical (governing equations discretization) and physical (sub-grid parameterizations) processes. The results for these calculations during the above mentioned SACZ event are summarized in **Table 3**. The application of any kind of nudging technique improved the overall representation of the SACZ, with applications using wave numbers associated with length scales of 2000 km or smaller showing minimum values for RMSD. Even though there are no larger differences between RMSD values displayed in **Table 3**, it is worth noticing that domain-wide length scales for the relaxation methods (*ndg8000*) do not seem to ensure better performance. Smaller values for RMSD are concentrated for experiments considering intermediate and smaller length scales.

3.2. Precipitation Fields

To evaluate the precipitation distribution generated by WRF experiments, results were compared to TRMM estimates. **Figure 9** shows the maps for accumulated rainfall during the event (top), the mapping RMSD values in comparison with the TRMM dataset during the event (middle) and the timeseries of RMSD values for the complete simulation period (bottom), from 26 November 2013 to 10 January 2014. It can be seen that, for the *ndgnone* experiment, there was some precipitation created, even though large-scale features related to the SACZ are not well formed. The total rainfall maps for this experiment do not indicate a SACZ formation and most of the precipitation

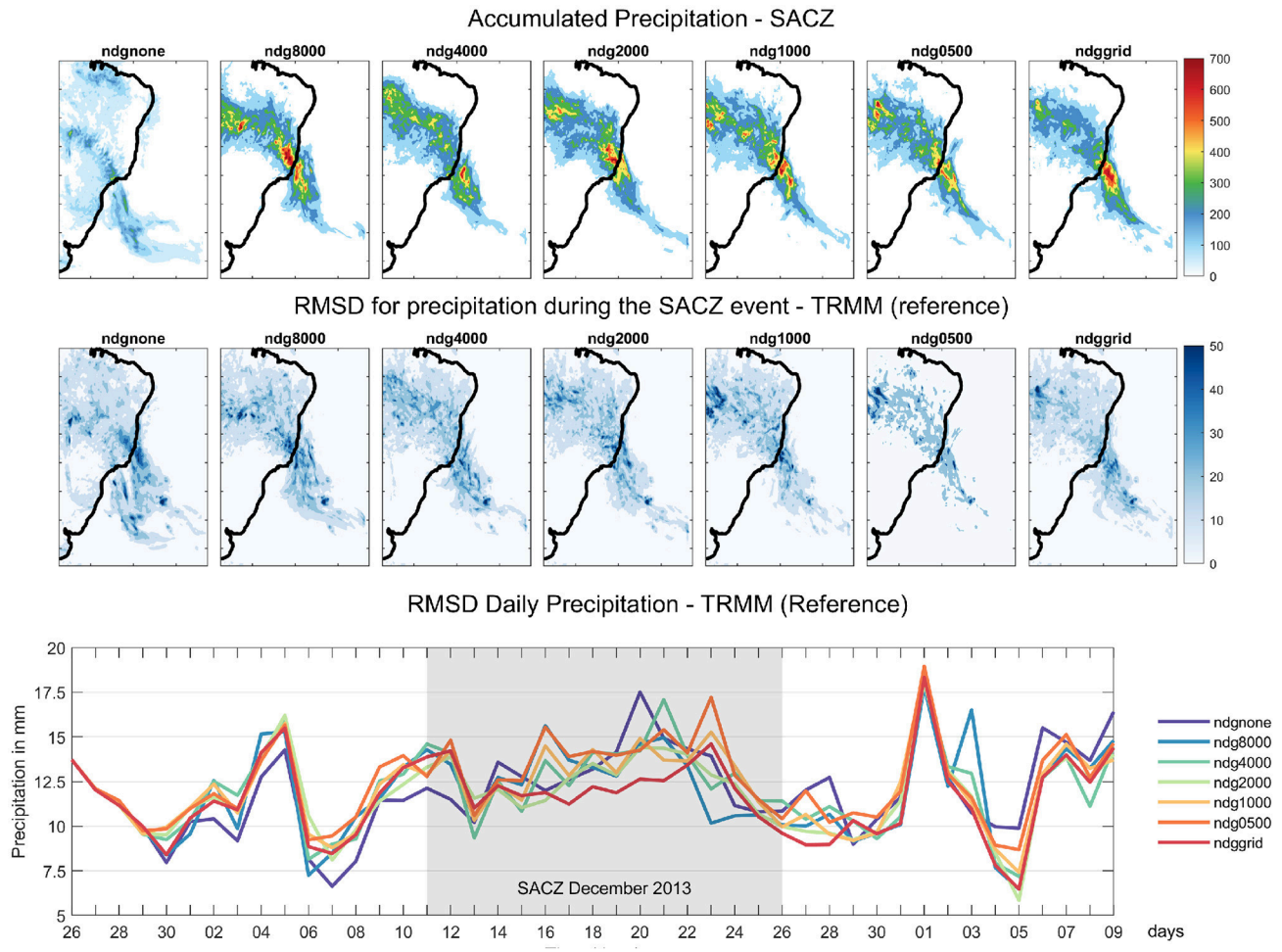

FIGURE 9 | Accumulated precipitation maps **(Top)** for all experiments during the SACZ event, RMSD maps for precipitation values during the SACZ event **(Middle)** and time series of RMSD values during the whole simulated period **(Bottom)**. All RMSD calculations are based on TRMM dataset as the observational reference.

occurs south of its average positioning with no projection of the Amazon branch of this feature. On the other hand, for all nudging experiments, the cumulative precipitation fields show great resemblance to the TRMM field and most differences between experiments seem related to highly convective centers in the Amazon branch of the SACZ.

The timeseries for the RMSD values (**Figure 9**, bottom) indicate that all experiments, with or without nudging, account for similar errors in the rainfall quantity. The maximum value for RMSD is found during the SACZ event (December 20) for the *ndgnone* test and exceeds all other experiments that used relaxation. The less pronounced values for RMSD in those cases are directly associated with the proper SACZ representation provided by the results, as detailed in previous sections. On the other hand, spatial distribution of the errors (RMSD maps, **Figure 9**, middle) can offer a better idea of the error spreading between experiments. Most of these faults occur over the Amazon and Oceanic branches of the SACZ, possibly related to the mesoscale representation by surface parameterizations. In **Figure 9** (middle), the RMSD is less pronounced for experiments using smaller wavelengths for the nudging application, especially over the western Amazonian area.

Overall, the use of nudging yielded in a better representation of the SACZ rainfall distribution, given the appropriate configuration of large-scale features essential for its development, as explored in earlier sections. Even though noticeable differences between nudged experiments can be found, all approaches led to a good representation of precipitation distribution over the SACZ main axis.

4. CONCLUSIONS

Several numerical experiments with the WRF model were conducted with different nudging options during an intense SACZ event in December 2013. This case was chosen given the intensity, persistence and significant damages related to the ongoing rainfall throughout the 15 days of activity. Since the SACZ events are driven directly by large scale atmospheric

features, the escalation of errors by internal modes can interfere with the its representation by introducing bias in those scales, specially for longer simulations. The use of spectral nudging can effectively improve the results by enforcing the model solution to follow the large-scale reference, while still allowing the dynamic and physical cores to contribute in the smaller scales solutions. In our experiments, all nudging experiments presented better performance in representing the features that anchor the SACZ. The spatial spectrum of kinetic energy and RMSD plots showed that nudging cases applied with higher wave numbers, correspondent to smaller lengths, improve the overall performance of simulation but may damp the solution from the physical and dynamical model cores.

Spatial fields of variables nudged that represent the SACZ structure show that any nudging application can yield to results with favorable large-scale features for the SACZ formation and persistence. Therefore, using a less restrictive option (lower wave numbers and larger scales filtered in the process) is ideal in this scenario. The *ndg2000* case (scale lengths of 2000 km) provides a reasonable balance between diminishing errors and restriction to the numerical solution provided by the mode.

This is corroborated by the precipitation distribution fields. Differences between nudged experiments suggest that the internal solutions generated by the model are sensible to the choice of a proper wave number. This result is also corroborated by previous studies (Miguez-Macho et al., 2004, 2005; Wang and Kotamarthi, 2013; Gómez and Miguez-Macho, 2017) that suggest using only wave numbers associated only with larger scales is enough to balance the large-scale representation and the internal contribution from the model dynamics and physical suites in the final solution. This can be particularly necessary for simulations of subseasonal scales.

AUTHOR CONTRIBUTIONS

NS designed and performed the numerical experiments and was responsible for the manuscript writing. RC provided critical revision to the procedures and manuscript, along with scientific advising.

ACKNOWLEDGMENTS

This study was supported by the Coordenação de Aperfeicoamento de Pessoal de Nível Superior (CAPES) and the Conselho Nacional de Desenvolvimento Científico e Tecnológico (CNPq,164184/2014-7).

REFERENCES

Bombardi, R. J., and Carvalho, L. M. V. (2011). The South Atlantic dipole and variations in the characteristics of the South American Monsoon in the WCRP-CMIP3 multi-model simulations. *Climate Dyn.* 36, 2091–2102. doi: 10.1007/s00382-010-0836-9

Carvalho, L. M. V., Silva, A. E., Jones, C., Liebmann, B., Silva Dias, P. L., and Rocha, H. R. (2011). Moisture transport and intraseasonal variability in the South America monsoon system. *Climate Dyn.* 36, 1865–1880. doi: 10.1007/s00382-010-0806-2

Collins, W. D., Rasch, P. J., Boville, B. A., Hack, J. J., McCaa, J. R., Williamson, D. L., et al. (2004). *Description of the NCAR Community Atmosphere Model (CAM 3.0)*. Techreport, National Center For Atmospheric Research.

da Silva, A. E., and de Carvalho, L. M. V. (2007). Large-scale index for South America Monsoon (LISAM). *Atmospher. Sci. Lett.* 8, 51–57. doi: 10.1002/asl.150

Davies, H. C. (1983). Limitations of some common lateral boundary schemes used in Regional NWP Models. *Month. Weath. Rev.* 111, 1002–1012. doi: 10.1175/1520-0493(1983)111<1002:LOSCLB>2.0.CO;2

Davies, H. C., and Turner, R. E. (1977). Updating prediction models by dynamical relaxation: an examination of the technique. *Q. J. R. Meteorol. Soc.* 103, 225–245. doi: 10.1002/qj.49710343602

de Quadro, M. F. L., Dias, M. A. F. D. S., Herdies, D. L., and de Gonçalves, L. G. G. (2012). Análise climatológica da precipitação e do transporte de umidade na região da ZCAS através da nova geração de reanálises. *Rev. Brasil. Meteorol.* 27, 152–162. doi: 10.1590/S0102-77862012000200004

Dee, D. P., Uppala, S. M., Simmons, A. J., Berrisford, P., Poli, P., Kobayashi, S., et al. (2011). The ERA-Interim reanalysis: configuration and performance of the data assimilation system. *Q. J. R. Meteorol. Soc.* 137, 553–597. doi: 10.1002/qj.828

Dickinson, R., Errico, R., Giorgi, F., and Bates, G. (1989). A regional climate model for the western United States. *Climat. Change* 15, 383–422. doi: 10.1007/BF00240465

Errico, R. M. (1985). Spectra computed from a limited area grid. *Month. Weath. Rev.* 113, 1554–1562. doi: 10.1175/1520-0493(1985)113<1554:SCFALA>2.0.CO;2

Gan, M. A., Rao, V. B., and Moscati, M. C. L. (2005). South American monsoon indices. *Atmospher. Sci. Lett.* 6, 219–223. doi: 10.1002/asl.119

Gómez, B., and Miguez-Macho, G. (2017). The impact of wave number selection and spin-up time in spectral nudging. *Q. J. R. Meteorol. Soc.* 143, 1772–1786. doi: 10.1002/qj.3032

Hong, S., and Lim, J.-O. J. (2006). The WRF single-moment 6-Class microphysics scheme (WSM6). *J. Korean Meteorol. Soc.* 42, 129–151.

Huffman, G. J., Bolvin, D. T., Nelkin, E. J., Wolff, D. B., Adler, R. F., Gu, G., et al. (2007). The TRMM multisatellite precipitation analysis (TMPA): Quasi-Global, multiyear, combined-Sensor precipitation estimates at fine scales. *J. Hydrometeorol.* 8, 38–55. doi: 10.1175/JHM560.1

Kain, J. S. (2004). The Kain–Fritsch convective parameterization: an update. *J. Appl. Meteorol.* 43, 170–181. doi: 10.1175/1520-0450(2004)043<0170:TKCPAU>2.0.CO;2

Kodama, Y. (1992). Large-scale common features of subtropical precipitation zones (the Baiu Frontal Zone, the SPCZ, and the SACZ) Part I: characteristics of subtropical frontal zones. *J. Meteorol. Soc. Jpn. II* 70, 813–836. doi: 10.2151/jmsj1965.70.4_813

Kodama, Y.-M. (1993). Large-Scale Common Features of Sub-Tropical Convergence Zones (the Baiu Frontal Zone, the SPCZ, and the SACZ) Part II : Conditions of the Circulations for Generating the STCZs. *J. Meteorol. Soc. Jpn. II* 71, 581–610. doi: 10.2151/jmsj1965.71.5_581

Marengo, J. A., Liebmann, B., Grimm, A. M., Misra, V., Silva Dias, P. L., Cavalcanti, I. F. A., et al. (2012). Recent developments on the South American monsoon system. *Int. J. Climatol.* 32, 1–21. doi: 10.1002/joc.2254

Miguez-Macho, G., Stenchikov, G. L., and Robock, A. (2004). Spectral nudging to eliminate the effects of domain position and geometry in regional climate model simulations. *J. Geophys. Res. Atmosph.* 109:D13104. doi: 10.1029/2003JD004495

Miguez-Macho, G., Stenchikov, G. L., and Robock, A. (2005). Regional climate simulations over North America: interaction of local processes with improved large-scale flow. *J. Clim.* 18, 1227–1246. doi: 10.1175/JCLI3369.1

Niu, G.-Y., Yang, Z.-L., Mitchell, K. E., Chen, F., Ek, M. B., Barlage, M., et al. (2011). The community Noah land surface model with multiparameterization options (Noah-MP): 1. Model description and evaluation with local-scale measurements. *J. Geophys. Res.* 116:D12109. doi: 10.1029/2010JD015139

Saha, S., Moorthi, S., Pan, H.-L., Wu, X., Wang, J., Nadiga, S., et al. (2010). The NCEP climate forecast system reanalysis. *Bull. Am. Meteorol. Soc.* 91, 1015–1058. doi: 10.1175/2010BAMS3001.1

Skamarock, W. C., and Klemp, J. B. (2008). A time-split nonhydrostatic atmospheric model for weather research and forecasting applications. *J. Comput. Phys.* 227, 3465–3485. doi: 10.1016/j.jcp.2007.01.037

Stauffer, D. R., and Seaman, N. L. (1990). Use of four-dimensional data assimilation in a limited-area Mesoscale Model. Part I: experiments with synoptic-scale data. *Month. Weath. Rev.* 118, 1250–1277. doi: 10.1175/1520-0493(1990)118<1250:UOFDDA>2.0.CO;2

Vera, C., Higgins, W., Amador, J., Ambrizzi, T., Garreaud, R., Gochis, D., et al. (2006). Toward a unified view of the American Monsoon Systems. *J. Clim.* 19, 4977–5000. doi: 10.1175/JCLI3896.1

Vincent, C. L., and Hahmann, A. N. (2015). The impact of grid and spectral nudging on the variance of the near-surface wind speed. *J. Appl. Meteorol. Climatol.* 54, 1021–1038. doi: 10.1175/JAMC-D-14-047.1

von Storch, H., Langenberg, H., and Feser, F. (2000). A spectral nudging technique for dynamical downscaling purposes. *Month. Weath. Rev.* 128, 3664–3673. doi: 10.1175/1520-0493(2000)128<3664:ASNTFD>2.0.CO;2

Waldron, K. M., Paegle, J., and Horel, J. D. (1996). Sensitivity of a spectrally filtered and nudged limited-area Model to Outer Model Options. *Month. Weath. Rev.* 124, 529–547. doi: 10.1175/1520-0493(1996)124<0529:SOASFA>2.0.CO;2

Wang, J., and Kotamarthi, V. R. (2013). Assessment of dynamical downscaling in near-surface fields with different spectral nudging approaches using the Nested Regional Climate Model (NRCM). *J. Appl. Meteorol. Climatol.* 52, 1576–1591. doi: 10.1175/JAMC-D-12-0302.1

Zhang, D., and Anthes, R. A. (1982). A High-Resolution Model of the planetary boundary layer–sensitivity tests and comparisons with SESAME-79 data. *J. Appl. Meteorol.* 21, 1594–1609. doi: 10.1175/1520-0450(1982)021<1594:AHRMOT>2.0.CO;2

Zhou, J., and Lau, K.-M. (1998). Does a monsoon climate exist over South America? *J. Clim.* 11, 1020–1040. doi: 10.1175/1520-0442(1998)011<1020:DAMCEO>2.0.CO;2

Conflict of Interest Statement: The authors declare that the research was conducted in the absence of any commercial or financial relationships that could be construed as a potential conflict of interest.